analytical chemistry

pubs.acs.org/ac Article

Expanding the Analytical Window for Biochar Speciation: Molecular Comparison of Solvent Extraction and Water-Soluble Fractions of Biochar by FT-ICR Mass Spectrometry

Amy M. McKenna,* Martha L. Chacón-Patiño, Huan Chen, Gregory T. Blakney, Frederic Mentink-Vigier, Robert B. Young, James A. Ippolito, and Thomas Borch

Cite This: *Anal. Chem.* 2021, 93, 15365−15372 Read Online

ACCESS | Metrics & More | Article Recommendations | Supporting Information

ABSTRACT: Biochar, a low-density yet carbon-rich material derived from different organic materials pyrolyzed under low or no oxygen conditions, has been widely studied as a soil amendment, for greenhouse gas mitigation and in remediation of trace element-contaminated soils. Molecular speciation of biochar compounds has been challenging due to low solubility, aggregation, and immense compositional polydispersity that challenges nearly all mass spectrometry methods routinely applied to carbon-based organic materials. Through a combined technique approach that applies advanced analytical strategies, we provide bulk and molecular characterization of Kentucky bluegrass biochar that can be applied to any biomass or biochar sample. First, we characterize Kentucky bluegrass biochar chemical functional groups by solid-state magic-angle spinning dynamic nuclear polarization NMR (MAS-DNP NMR) and resolve aromatic and aliphatic signals from the pyrogenic material and intact plant material. Next, we isolate water-soluble biochar species by solid-phase extraction followed by Fourier transform ion cyclotron resonance mass spectrometry (FT-ICR MS) and identify highly polar, oxygen species across a wide carbon number range. Solvent fractionation of biochar further expands the compositional range and identifies condensed polycyclic aromatic species across nonpolar and polar classes detected by two ionization modes (-ESI and +APPI) by FT-ICR MS. Plotting biochar species with DBE versus carbon number highlights the pericondensed molecular structural motif that persists across numerous heteroatom classes and ionization modes. To the best of our knowledge, this is the first molecular level identification of nonfunctionalized PAHs in biochar extracts by APPI FT-ICR MS. Thus, we identify biochar species that span the same compositional space as coal, heavy oil asphaltenes, and coal tar and correspond to condensed ring PAHs.

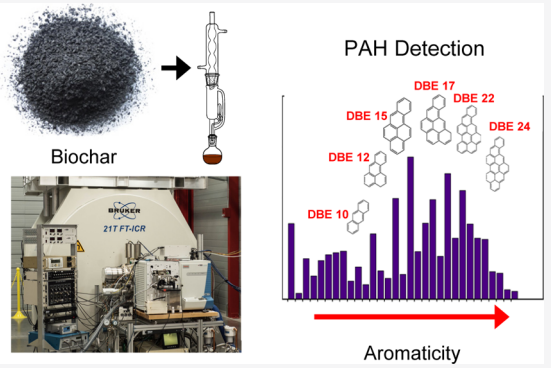

INTRODUCTION

Biochar produced from plant and biomass materials (e.g., grass, agricultural, and forest residues) decomposed at high temperatures is a complex, highly porous, carbon-rich material that has shown potential to increase the water-holding capacity of soils and increase soil cation exchange capacity and plant nutrient-absorbing ability. Additionally, biochar application in agricultural practices has numerous advantages, including improving soil quality, mitigating greenhouse gas emissions, increasing crop productivity, and augmentation of soil carbon storage.[1−3] Biochar derived from different organic materials has potential use in remediation and restoration of trace element-, organic pollutant-, and crude oil-contaminated soils.[4] Substantial research on biochar as a soil amendment to reduce adverse trace element impacts on plant and human health has increased in recent years due to the capacity of biochar to influence trace element biogeochemical cycling or by functioning as a sorbent for environmental contamination remediation.[4,5] Plant uptake on trace elements depends on both soil and biochar properties, and studies have evaluated the potential of biochar to diminish human health hazards due to consuming trace element-contaminated food.

However, during the pyrolytic conversion of biomass below 500 °C, toxic organic pollutants (e.g., polycyclic aromatic hydrocarbons, PAHs) are often formed and reside in and on biochar residues.[1,5] PAHs in biochar are formed through degradation of lignin and cellulose through dealkylation, dehydrogenation, cyclization, aromatization, and/or radical reactions that eliminate functional groups (e.g., H_2O, CO_2, CH_4, and H_2S), leaving behind low- and high-molecular weight

Received: July 20, 2021
Accepted: October 27, 2021
Published: November 11, 2021

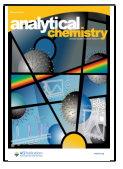

https://doi.org/10.1021/acs.analchem.1c03058
Anal. Chem. 2021, 93, 15365−15372

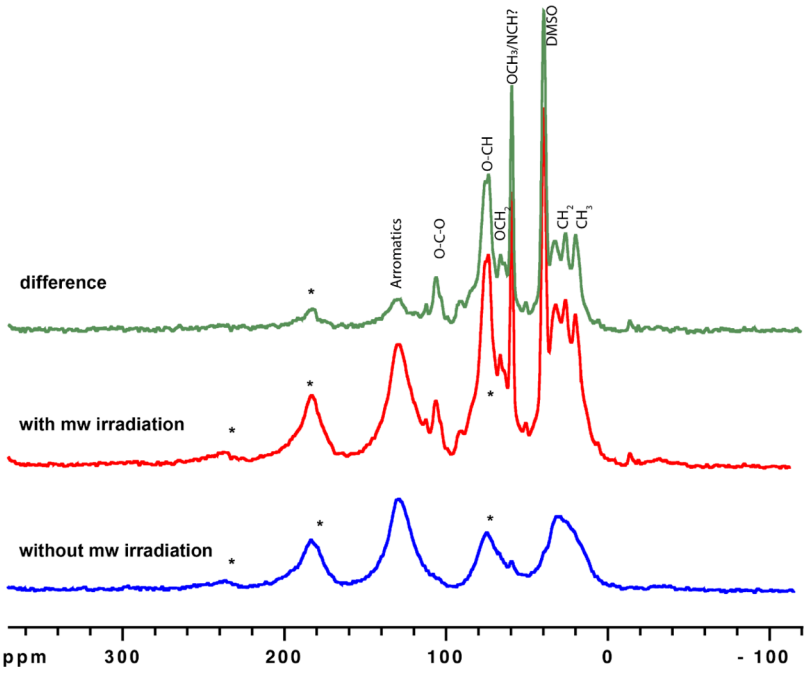

Figure 1. ^{13}C CP solid-state NMR spectra performed in a 600 MHz/14.1 T solid-state NMR spectrometer equipped with a 395 GHz gyrotron microwave source for MAS-DNP or Kentucky bluegrass impregnated with 10 mM AsymPolPOK (asymmetric bis-nitroxides, in which a piperidine-based radical and pyrrolinoxyl or a proxy radical are linked together).[33] Blue corresponds to the signal without microwave irradiation, red is with irradiation, and green is the difference spectrum between red and blue. * represents the spinning sidebands.

aromatic structures.[6] Below 300 °C, small PAHs are formed, and three or four ring structures form between 300 and 600 °C.[7−9] Above 500 °C, larger PAHs are formed through a free radical pathway followed by pyrosynthesis.[10] Several studies characterized the toxicity and molecular composition of water-soluble biochar compounds derived from biochar derived from different feeds and pyrolysis temperatures and show wide variability in dissolved organic and inorganic compositions that inhibit aquatic organism growth.[2] Importantly, these studies highlight the need for biochar materials to be free of toxic compounds.[6,11]

Environmental impact of widespread biochar application includes the potential for introducing PAHs and other contamination to soils.[12,13] However, condensed aromatic systems are very difficult to detect and characterize, although numerous studies have detected aromatic species in biochar by one-dimensional nuclear magnetic resonance and hypothesized chemical functionality.[14−16] Aromatic groups reported in biochar by two-dimensional solid-state NMR and FT-IR from various biomass feeds (e.g., cellulose, lignin, tannin, and whole biomasses such as pine wood, pine residue, and pine bark)[17] and organic feedstocks[16,18] (e.g., wood chips and organic urban waste) appear to originate from condensed aromatics.[15−17] However, identification of condensed aromatics using NMR/FTIR techniques is extremely difficult and requires very complex pulse programs.[19−21]

The polydispersity, polyfunctionality, and compositional complexity of biochar require resolving power sufficient to separate species that differ in mass by the mass of an electron across a wide molecular weight range, only achievable with Fourier transform ion cyclotron resonance mass spectrometry.[22,23] Aqueous extraction of biochar captures the mobile fraction of biochar in soil systems that can be further characterized by mass spectrometry.[24] Charcoal produced in wildfire-impacted soils form pyrogenic DOM (pyDOM, which includes soot, black carbon, biochar, and charcoal)[25] after mixing with water (e.g., rainfall) and has been used to estimate fluxes of pyDOM in rivers, determine what type of molecules leach into the environment, and interrogate both abiotic (photochemical) and biotic (microbial) degradation pathways.[14,26] Organic solvents recover the highest amount of material from organic matter detected using GC-based techniques but are limited to species within the GC volatility window.[13]

PyDOM, charcoals, soots, and biochars have limited aqueous solubility. Solvent fractionation often employs Soxhlet extraction, which does not require filtration and is not matrix-dependent, summarized by Wang et al.[9] Many studies rely on Hilber et al.[27] and Fabbri et al.,[28] which report the highest recovery of 16 U.S. EPA PAHs in biochar with 100% toluene over a 36 h Soxhlet extraction. Solvent fractionation widely used for heavy oil characterization isolates specific chemical functional groups. For example, acetone has been reported for the selective removal of small/pericondensed aromatic (1−4 fused rings) as a result of its moderate solvent strength for PAHs.[29] Tetrahydrofuran (THF) has shown promise in recovering condensed rings and polar compounds from aggregated petroleum fractions (asphaltenes).[30] Methanol has widely been used for isolation of polar species from a host of carbon matrices, including DOM, SOM, and biochar.[31]

We approach biochar as a highly complex, polyfunctional, and polydisperse aggregated mixture of organic molecules and apply extraction and data visualization methods that can discern structural trends relevant for environmental applications. We report a solvent fractionation method designed to dissociate aggregated species in biochar and compare the molecular composition of WSO-derived species to that of solvent-derived species across two ionization modes by FT-ICR MS. Here, nonfunctionalized PAHs in biochar are identified for the first time by APPI FT-ICR MS. Importantly,

https://doi.org/10.1021/acs.analchem.1c03058
Anal. Chem. 2021, 93, 15365−15372

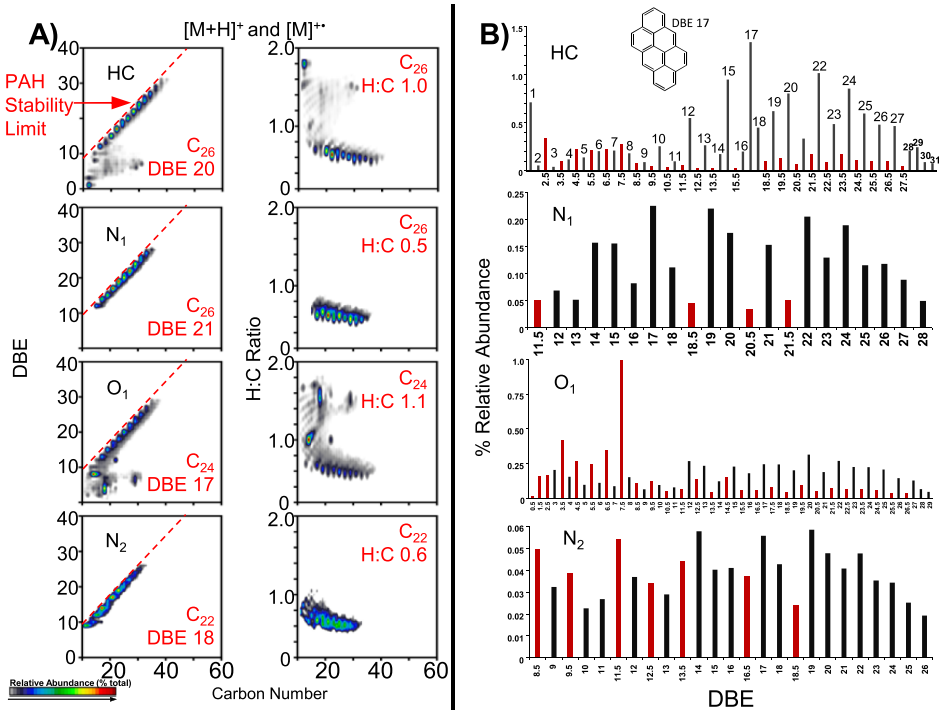

Figure 2. (A) Isoabundance color-coded contoured plots of DBE versus carbon number for hydrocarbon (HC), N_1, O_1, and N_2 classes derived from positive-ion APPI FT-ICR MS. The relative abundance-weighted average DBE, carbon number, and H/C ratio are shown for each image. The PAH planar stability limit line is denoted by a red dashed line in each DBE versus carbon number image to highlight the lack of alkylation on detected species. (B) DBE distribution for each heteroatom class. Half-integer DBE values correspond to protonated species, whereas whole integer DBE values correspond to radical cations formed by APPI.

visualization of each specific heteroatom class through plots of aromaticity (double bond equivalents, DBE, number of rings plus double bonds to carbon) versus carbon number reveals aromatic structural motifs across both nonpolar and polar classes observed in both negative-ion ESI and positive-ion APPI for solvent extractions of biochar.

EXPERIMENTAL METHODS

All experimental methods (biochar preparation, isolation of water-soluble organics, solvent fractionation, and complete FT-ICR MS details) are fully detailed in the Supporting Information.

RESULTS AND DISCUSSION

MAS-DNP NMR Identifies Aromatics in Biochar. To identify chemical functional groups in Kentucky bluegrass biochar, we apply solid-state ^{13}C MAS-DNP NMR, a method that increases the sensitivity of ssNMR by orders of magnitude.[32] The biochar sample was impregnated with a 10 mM solution of the biradical AsymPolPOK73 and then inserted in a probe cooled down to 100 K. The sample was subsequently irradiated with a microwave source to enable the transfer of polarization from the biradicals to hydrogen nuclei. Figure 1 shows ^{13}C CP solid-state NMR spectra performed in a 600 MHz/14.1 T solid-state NMR spectrometer.[33] The bottom (blue spectrum) represents the NMR spectrum in the absence of microwave irradiation and reports the presence of aromatic and aliphatic ^{13}C signals, which are centered at around 130 ppm and 30 ppm, respectively. The signals are broad and featureless and illustrate a wide distribution of chemical sites that remain unresolved due to polydispersity. The middle (red spectrum) corresponds to the MAS-DNP-enhanced ssNMR spectrum and shows more resolved features that correspond to carbohydrates (75−105 ppm) found in cellulose/hemi-cellulose and also aliphatic carbon (20−50 ppm), in addition to the same aromatic and aliphatic signals observed without microwave irradiation. The broad aromatic and aliphatic components are not enhanced with microwave irradiation, although the carbohydrate/resolved aliphatic carbon signals are enhanced by a factor of >30. This is further highlighted in the top (green) spectrum, which corresponds to the difference spectrum with and without microwave irradiation and highlights the signals enhanced by the DNP process (i.e., carbohydrate and protein-like signals). The broad aromatic and aliphatic regions may not be enhanced due to their shorter relaxation times as compared to the other signal (~3 s). These shorter relaxation times (<2 s) may originate from intrinsic unpaired electron spins commonly found in materials like coal.[34] The Kentucky bluegrass biochar sample consists of disordered aromatic- and aliphatic-containing compounds (coal) with a small fraction of intact plant material via MAS-DNP.

APPI FT-ICR MS Identifies Nonpolar Aromatic Species in Biochar in the Acetone/Cyclohexane Fraction. *Heteroatom Class Distribution.* The heteroatom class distribution derived from positive-ion APPI FT-ICR MS analysis for the acetone/cyclohexane fraction of Kentucky bluegrass biochar is shown in Figure S1, shown as percent relative abundance for each class, scaled to the 100% peak in each mass spectrum. The most abundant class corresponds to hydrocarbon (HC), O_1, O_2, and O_3 classes. N_1, N_2, and N_3 species are also detected by positive-ion APPI and likely correspond to pyridinic nitrogen (N_1) with the second and

https://doi.org/10.1021/acs.analchem.1c03058
Anal. Chem. 2021, 93, 15365−15372

third nitrogen in the form of either pyrrolic or pyridinic nitrogen.

DBE versus Carbon Number Images Reveal Condensed Aromatic Structural Motifs. APPI FT-ICR MS identifies 5,221 unique, monoisotopic molecular formulas in the acetone/cyclohexane fraction, with the most abundant species corresponding to nonpolar hydrocarbon species. This indicates that biochar contains hydrocarbons not as efficiently ionized by ESI as oxygen-containing species.[35] However, isoabundance color-coded contoured plots of DBE (double bond equivalents, the number of rings plus double bonds to carbon, DBE = $C - h/2 + n/2 + 1$) versus carbon number allow visualization of the most abundant core structures within a specific heteroatom class for each ionization mode and represent a new way to highlight specific structural trends in NOM and readily identify misassigned species.[36] In addition, DBE versus carbon number images allow for compositional comparison of nonpolar classes (i.e., species that do not contain oxygen), highlight core structures for a heteroatom class, are unique to van Krevelen diagrams that plot H/C versus O/C, and ignore nonoxygen-containing classes. Plotting biochar species as DBE versus carbon number highlights the pericondensed molecular structural motif that persists across numerous heteroatom classes and across multiple ionization modes. Plots of DBE versus carbon number for the hydrocarbon (HC), N_1, O_1, and N_2 classes derived from positive-ion APPI FT-ICR MS of the acetone/cyclohexane fraction are shown in Figure 2a. We selected these classes to highlight novel classes not detected by other ionization modes. The relative abundance-weighted average carbon number, DBE, and H/C ratio are shown in each image, calculated from neutral elemental compositions.

Across all classes, identified species correspond to DBE values between 1 and 30, and the carbon number ranges from C_{10} to C_{40}, with 2−4 CH_2 units per homologous series (species with equal DBE but varying carbon numbers). This indicates the prevalence of aromatic molecules with 4−8 rings per system with limited alkyl substitution (short alkyl chains). The most abundant DBE for the hydrocarbon class is DBE 17, with the most abundant species of $C_{22}H_{12}$. This elemental composition matches that of anthanthrene (naphtho-[7,8,1,2,3-*nopqr*]tetraphene), a six-ring condensed ring system, one of over 100 PAHs formed during incomplete burning of organic substances, and a food toxin and pollutant. Figure S3 highlights core structures and elemental compositions of PAHs detected in the hydrocarbon fraction by +APPI, with ring systems ranging from 4 rings (pyrene) to 10 rings (pentacene). This result agrees with previous reports of thermogenic signatures of deep-sea DOM isolated by SPE-PPL from hydrothermal vents identified by ESI FT-ICR MS that report ∼7 ring PAH systems that the authors conclude to be derived from petrogenic sources.[37] Here, we identify core aromatic structures across a wide molecular weight range ($200 < m/z < 850$) in biochar solvent extracts that span nonpolar and oxygen-containing species by +APPI FT-ICR MS.

DBE Distribution. DBE distributions are shown in Figure 2b to highlight the most abundant DBE class for each heteroatom class to show the DBE "hotspots", with each class containing species with more than 28 DBE. Figure 2b shows the DBE distribution for the data shown in Figure 2a in a two-dimensional plot of percent relative abundance versus DBE for each heteroatom class. Protonated molecules (red) have half-integer DBE values (DBE = $c - h/2 + n/2 + 1$, calculated from the ion elemental composition, $C_cH_hN_nO_oS_s$) and may thus be distinguished with radical cations (black) with calculated integer DBE values. The most abundant DBE values correspond to integer DBE values for the hydrocarbon and N_1 class. Figure S2 shows potential core structures for the hydrocarbons detected that correspond to the most abundant DBE values. The relative abundance-weighted averaged carbon number, DBE, and H/C ratio for neutral elemental compositions (for protonated and radical cations) are shown in each image. Because APPI results in two ion types, both protonated and radical cation species are plotted in one compositional image.[38] Across all three classes, biochar species correspond to pericondensed ring aromatic structures with detected carbon number distributions averaging between ∼ C_{22} and C_{26}. Experimental m/z, elemental composition, DBE, and mass error for radical cations (Table S1) and protonated species (Table S2) were detected in all four classes. A complete list of all mass spectral peak assignments can be found in the repository link at the end of the manuscript. Collectively, these results indicate that Kentucky bluegrass biochar contains species that correspond to elemental compositions that match the molecular formula of known PAHs.

PAH Planar Stability Limit. Aromaticity (hydrogen deficiency, represented as the DBE or H/C ratio) of polycyclic aromatic hydrocarbons (PAHs) cannot exceed a maximum value for a given carbon number, which increases linearly with increasing the carbon number. Biochar species extracted with acetone/cyclohexane detected by positive APPI FT-ICR MS shown in Figure 2a consist of condensed PAH systems that approach the theoretical limit (dashed line) for stable planar PAHs. Representative core structures for hydrocarbons are shown in Figure S2, and elemental compositions for select m/z are shown in Table S2. Aromaticity above the planar stability limit (e.g., PAH limit, DBE value above the red line at a given carbon number) requires "buckybowl"-type structures (convex−concave pi-conjugated surfaces in hemispherical structures, e.g., corannulene)[39] reported as intermediate molecules in petroleum catalytic cracking[40] but have not been reported in pyrogenic biomass.[41] We apply this upper boundary to readily identify the degree of condensation (i.e., peri- vs catacondensed)[42] for aromatic species. Importantly, plotting the data in DBE versus carbon number images shows that elemental compositions for biochar species correspond to highly pericondensed/alkyl-depleted aromatic structures, similar to coal, coal tar, and heavy oil asphaltenes.

H/C versus Carbon Number. Because FT-ICR MS results in elemental composition assignments, data shown in Figure 2a (left) can be replotted as the H/C ratio versus carbon number (right) to compare the molecular composition of each heteroatom class to biochar bulk properties reported using other techniques.[43] Across all four classes shown, the relative abundance-weighted average H/C ratio is less than 1.0, which indicates greater fused aromatic ring structures due to thermochemical alteration.[43] Hydrocarbon and N_1 species report H/C values of 0.5−0.6, which could indicate preferential modification based on the heteroatom content.

Negative-Ion ESI of Solvent Extracts Reveals Condensed Aromatic Species in Biochar Not Detected by WSO-SPE. *Heteroatom Class Distribution Comparison of WSO-SPE and Solvent Extracts.* Negative-ion ESI of water-soluble components of biochar is a predominant method in the literature for molecular identification by FT-ICR MS. Therefore, we compare negative ESI from both WSO-SPE isolates with solvent extracts by FT-ICR MS. Figure S3 shows

https://doi.org/10.1021/acs.analchem.1c03058
Anal. Chem. 2021, 93, 15365−15372

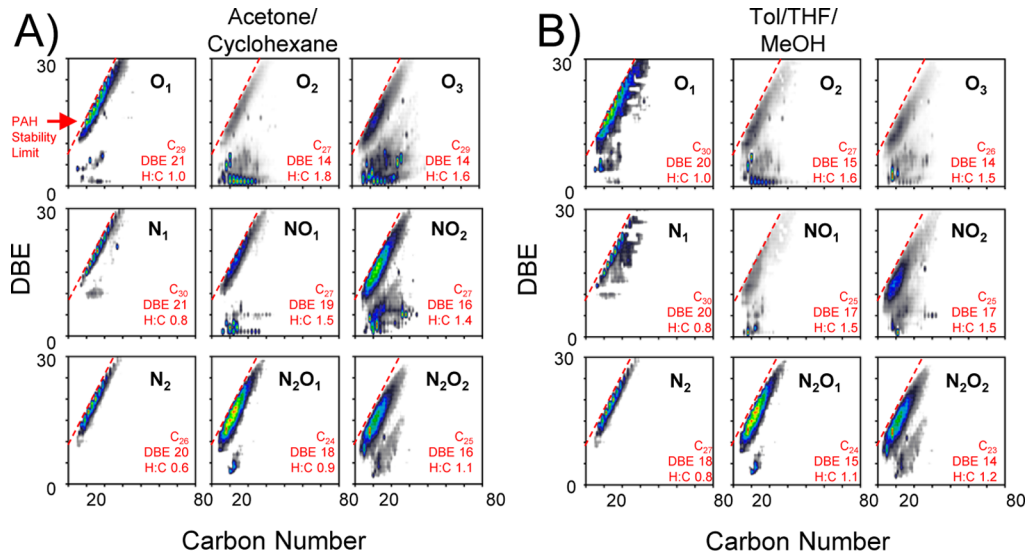

Figure 3. Heteroatom compound class distribution for water-soluble organic biochar species isolated by solid-phase extraction (blue) and species isolated by Soxhlet extraction with acetone/cyclohexane (red) and toluene/tetrahydrofuran/methanol (green) derived from negative-ion electrospray ionization FT-ICR MS at 21 T, showing O_x, N_1O_x, N_2O_x, and N_3O_x compounds for three fractionation techniques. Species that contain only carbon and hydrogen (HC) are detected in negative-ion ESI, corresponding to five-member ring hydrocarbons.

heteroatom classes detected in WSO, acetone/cyclohexane, and Tol/THF/MeOH extracts of Kentucky bluegrass biochar by negative-ion ESI FT-ICR MS. WSO-SPE and solvent fractions span a wide range of O_x, N_1O_x, N_2O_x, and N_3O_x classes. The most abundant acidic class in the WSO-SPE extract corresponds to O_7-O_9, which corresponds to compounds that contain at least one carboxylic acid moiety, with up to 19 oxygens per molecule (O_{19}), and multiple condensed ring species.[44] A similar trend is observed for WSO nitrogen-containing classes isolated by SPE, with nitrogen species detected with up to 14 and 16 oxygens (N_1O_{18}, N_2O_{16}, and N_3O_{14}). Importantly, Soxhlet extraction identifies nonpolar hydrocarbon, abundant O_1 species, and weakly acidic/neutral nitrogen N_1, N_2, and N_3 classes not identified in WSO-SPE.[45,46] In negative-ion ESI, unsubstituted N_1 species are formed through deprotonation to yield $[M-H]^-$ ions, which correspond to five-member pyrrolic nitrogen, detected by NMR in pyrolysis fractions of dissolved organic matter, Arctic watersheds, deep oceans, and forest soils. However, these techniques cannot identify specific molecular species associated with nitrogen structures. Pyrrole is a weakly acidic, neutral nitrogen compound (pK_a = 17.5) due to the presence of an imino hydrogen atom detected in petroleum that does not efficiently partition into water and is not detected in biochar WSO. Substituted pyrrolic species have been reported in biochar from *N*-doped biomass, and nitrogen-containing biochar is used for sorption of aromatic species from PAH-contaminated soils. Species that contain more than one nitrogen by negative ESI (i.e., N_2 or N_3 classes) contain at least one pyrrolic nitrogen where deprotonation occurs and have been identified in numerous petroleum-derived samples.[35] We report molecular identification of unsubstituted N_1, N_2, and N_3 species in biochar-derived samples by negative-ion ESI FT-ICR MS. These species are not detected in the WSO-PPL likely due to decreased water solubility, and we conclude that these species are more "oil-like" (condensed aromatics with little to no alkylation) than "NOM-like", and thus, we approach this analytically from an oil-focused approach. We detect N_1-N_3 species by negative-ion ESI for the first time in biochar.[47]

Hydrocarbons Detected in Biochar. Hydrocarbons detected by negative ESI correspond to five-member ring polycyclic compounds that contain at least one central five-membered ring fused to a flanking six-member aromatic ring, such as C-9 in fluorene, where deprotonation occurs. However, positive-ion APPI targets aromatic structures, and hydrocarbons detected in biochar extracts can correspond to saturated rings or aromatic five- and/or six-membered ring aromatic structures. Therefore, selective ionization of five-member ring hydrocarbons by negative ESI identifies lower DBE hydrocarbon structures that are less efficiently ionized than higher DBE hydrocarbon structures.

Comparison of the Compositional Space: WSO and Solvent-Extracted Acids of Biochar. Figure S4 shows the isoabundance color-contoured plot of DBE versus carbon number images for the oxygen classes detected by negative ESI FT-ICR MS in the WSO (top), acetone/cyclohexane (middle), and toluene/THF/MeOH (bottom) fractions and shows relative abundance-weighted average DBE and carbon number, calculated from neutral elemental compositions. Across the same heteroatom class, water-soluble biochar species correspond to lower DBE and lower carbon number compounds compared to solvent extracts, in agreement with previous reports for grass-derived biochar aqueous extracts.[48] Surprisingly, acidic species in acetone/cyclohexane and Tol/THF/MeOH extracts reveal a bimodal distribution in the compositional space: a higher DBE/lower carbon number distribution spans a similar compositional space as WSO species with a second distribution across a lower DBE/higher carbon number than WSO species.

The lower DBE, higher carbon number species in the solvent extract corresponds to more aliphatic compounds (higher H/C ratio). For the O_3 class, the O/C ratio decreases to 0.14, approximately half the O/C in O_7-O_{11} classes and extends to a higher carbon number. Importantly, the molecular species identified by ESI FT-ICR MS isolated through solvent extraction agree with atomic H/C and O/C ratios for biochar

https://doi.org/10.1021/acs.analchem.1c03058
Anal. Chem. 2021, 93, 15365−15372

produced between 500 and 599 °C and likely would change with feedstock, pyrolysis temperature, and the type of biochar.[43] Across all oxygen-containing classes, both acetone/cyclohexane and Tol/THF/MeOH species are lower in the O/C ratio and higher in the carbon number compared to WSO species and agree more closely with bulk atomic elemental ratios.[43] The trend toward an increased H/C ratio and carbon number for solvent-extracted molecules increases hydrophobicity that decreases water solubility and thus limits detection in WSO SPE-PPL. A similar trend is observed in the N_1O_x and N_2O_x classes (Figures S5 and S6). Here, we emphasize the comparison of two fractionation methods of one biochar that enable subsequent molecular speciation across a range of polarity. Additional biochar samples, pyrolysis conditions, and feedstock will be examined with this new two-step method as the focus of future studies.

Representative core structures for selected DBE values detected in acetone/cyclohexane fractions are shown in Figure S7. Experimental *m/z*, neutral elemental composition, mass error, and the DBE value for the corresponding O_1, N_1, N_1O_1, and N_2 acidic species are listed in Table S3.

Negative-Ion ESI and Solvent Extraction Reveal Condensed Aromatic Structures Not Detected by WSO-PPL. DBE versus carbon number images for several heteroatom classes only detected in solvent extracts (and not in WSO-PPL) are shown in Figure 3 (note: O_3 is included but was also detected in WSO). Acetone/cyclohexane-extracted acidic species in the O_1 class likely correspond to alcohols or furans and span a similar DBE and carbon number range for both fractions. N_1 species detected in negative-ion ESI can correspond to pyrrolic (five-member ring) nitrogen, where deprotonation can occur. In addition, azaarene congeners (nitrogen-heterocyclic polyaromatic pollutants) co-occur with PAHs in contaminated soils as reported by HPLC-qTOF MS, which identifies four- and five-ring azaarenes, known toxic and carcinogenic species (e.g., benzo[*c*]acridine and dibenzo[*a,h*]-acridine) in PAH-contaminated sites. Extracted acidic species contain approximately the same carbon number, DBE, and H/C ratio in both solvent mixtures. Pyrrolic nitrogen has been reported in fractions of DOM by solid-state ^{15}N NMR and X-ray photoelectron spectroscopy.[49] However, reports of pyrrolic nitrogen in biochar are limited to oxygen-containing species based on NMR and only report CHNO species by FT-ICR MS.[50] Across all classes with two or less heteroatoms per molecule, condensed ring aromatic species with minimal alkylation are detected in solvent extracts that are absent in the water-soluble fraction of biochar. In addition, when oxygen is present (e.g., N_2O_1 and N_2O_2), the compositional range increases in the carbon number, suggesting that structural diversity and alkyl content increase with oxygen incorporation. This is the first molecular identification of N_1 and N_2 acidic species in biochar and the first step in understanding the environmental implications.

Van Krevelen Diagrams of Acidic Species. Another way to rapidly visualize the tens of thousands of species derived from FT-ICR MS of complex organic mixtures like biochar is the van Krevelen diagram, which highlights global shifts in the H/C ratio (*y*-axis) and O/C ratio (*x*-axis) for all oxygen-containing species. Molecular formulas with similar features fall within a specific region and allow for comparison of compositional changes between samples. Each dot on the graph represents H/C and O/C ratios of elemental compositions derived from each mass spectrum. Smith et al.[11] determined through toxicological assays with biochar water extracts that the most toxic compounds contain negatively charged functional groups (e.g., carboxyl and hydroxyl groups) that fall within the lignin region on a van Krevelen diagram (H/C 0.7−1.5 and O/C 0.1−0.67).[51] Figure 4 is composed of the van Krevelen diagrams of the oxygen-

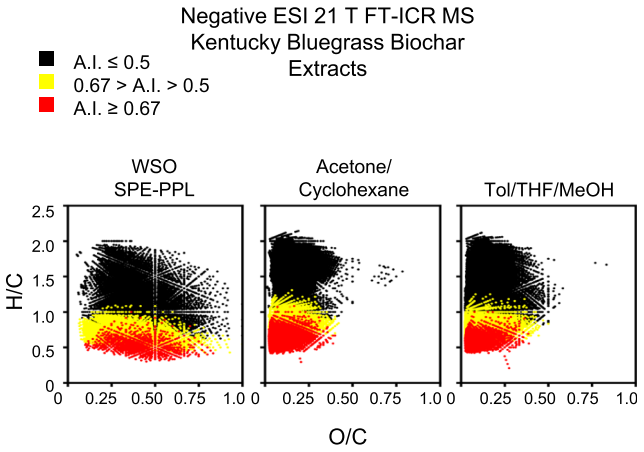

Figure 4. Van Krevelen diagrams of the H/C ratio versus O/C ratio for molecular formulae of oxygen species derived from negative-ion ESI FT-ICR MS for water-soluble species isolated by SPE-PPL (left) and solvent extraction with acetone/cyclohexane (center) and toluene/tetrahydrofuran/methanol (right). The aromaticity index corresponds to the degree of aromaticity based on elemental compositions.

containing acidic species detected in the water-soluble extract (left), acetone/cyclohexane (middle), and toluene/THF/MeOH (right) from Kentucky bluegrass biochar. Species with low O/C are highlighted in red, and those with moderate O/C are highlighted in yellow and high O/C are highlighted in black for rapid visual comparison of species detected across all three samples. Oxygen-containing species span approximately the same H/C ratio across all three samples (H/C ratio ∼0.5−2.0), with WSO species corresponding to slightly lower H/C (∼0.3) between O/C 0.3 and 0.6. Oxygen-containing species extracted with acetone/cyclohexane span an O/C ratio of 0.1−0.5, whereas more polar compounds with a higher O/C ratio are extracted with Tol/THF/MeOH, and species extend to an O/C ratio of 0.55. Both acetone/cyclohexane- and Tol/THF/MeOH-extracted species contain unsaturated (H/C 0.6−1.5 and O/C < 0.1) and lipid-like species (H/C 1.5−2.25 and O/C < 0.2) that are not detected in the WSO extract. Importantly, solvent extracts of biochar agree more closely with atomic elemental ratios of biochar that has been incompletely pyrolyzed and also agree with the ss-^{13} C NMR for Kentucky bluegrass biochar.[43]

CONCLUSIONS

We compare the molecular signature of water-soluble biochar species with that of solvent-extracted biochar species and identify and reveal highly condensed substituted and unsubstituted PAHs across a wide range of heteroatom classes and functionalities by FT-ICR MS. Several core structures correspond to known toxic PAHs (e.g., coronene), listed by the EPA as carcinogens. We focus here on one widely used biochar for agricultural systems to highlight the need for a multidisciplinary approach to identify species that could have

https://doi.org/10.1021/acs.analchem.1c03058
Anal. Chem. 2021, 93, 15365−15372

deleterious effects on the environment. All datasets shown herein are publicly available via the open science framework at https://osf.io/fg7hj/(DOI 10.17605/OSF.IO/FG7HJ).

■ ASSOCIATED CONTENT

Supporting Information

The Supporting Information is available free of charge at https://pubs.acs.org/doi/10.1021/acs.analchem.1c03058.

Biochar preparation, isolation of water-soluble organics, solvent fractionation, and data analysis (PDF)

■ AUTHOR INFORMATION

Corresponding Author

Amy M. McKenna − *Ion Cyclotron Resonance Facility, Florida State University, National High Magnetic Field Laboratory, Tallahassee, Florida 32310-4005, United States; Department of Soil and Crop Sciences, Colorado State University, Fort Collins, Colorado 80523-1170, United States;* orcid.org/0000-0001-7213-521X; Phone: 1 850 644 4809; Email: mckenna@magnet.fsu.edu; Fax: 1 850 644 1366

Authors

Martha L. Chacón-Patiño − *Ion Cyclotron Resonance Facility, Florida State University, National High Magnetic Field Laboratory, Tallahassee, Florida 32310-4005, United States;* orcid.org/0000-0002-7273-5343

Huan Chen − *Ion Cyclotron Resonance Facility, Florida State University, National High Magnetic Field Laboratory, Tallahassee, Florida 32310-4005, United States;* orcid.org/0000-0002-6032-6569

Gregory T. Blakney − *Ion Cyclotron Resonance Facility, Florida State University, National High Magnetic Field Laboratory, Tallahassee, Florida 32310-4005, United States;* orcid.org/0000-0002-4205-9866

Frederic Mentink-Vigier − *Nuclear Magnetic Resonance Facility, Florida State University, National High Magnetic Field Laboratory, Tallahassee, Florida 32310-4005, United States;* orcid.org/0000-0002-3570-9787

Robert B. Young − *Chemical Analysis & Instrumentation Laboratory, New Mexico State University, Las Cruces NM 88003, United States*

James A. Ippolito − *Department of Soil and Crop Sciences, Colorado State University, Fort Collins, Colorado 80523-1170, United States*

Thomas Borch − *Department of Soil and Crop Sciences, Colorado State University, Fort Collins, Colorado 80523-1170, United States; Department of Chemistry, Colorado State University, Fort Collins, Colorado 80523, United States;* orcid.org/0000-0002-4251-1613

Complete contact information is available at: https://pubs.acs.org/10.1021/acs.analchem.1c03058

Notes

The authors declare no competing financial interest.

■ ACKNOWLEDGMENTS

The authors thank Christopher L. Hendrickson, Chad R. Weisbrod, and John P. Quinn for design and maintenance of the 9.4 T and 21 T instruments. This work was supported by the NSF Division of Chemistry and Division of Materials Research through DMR-1644779 and the State of Florida. The authors also acknowledge support to T.B. from the National Science Foundation under grant number 1512670 and the USDA National Institute of Food Agriculture through AFRI grant no. 2021−67019034608 and support to J.I. through the USDA National Institute of Food and Agriculture, Multi-State Hatch project COL00292D, accession 1020695.

■ REFERENCES

(1) Odinga, E. S.; Waigi, M. G.; Gudda, F. O.; Wang, J.; Yang, B.; Hu, X.; Li, S.; Gao, Y. *Environ. Int.* **2020**, *134*, 105172.

(2) Odinga, E. S.; Gudda, F. O.; Waigi, M. G.; Wang, J.; Gao, Y. *Fundam. Res.* **2021**, *1*, 296−305.

(3) Gómez, N.; Rosas, J. G.; Singh, S.; Ross, A. B.; Sánchez, M. E.; Cara, J. *J. Anal. Appl. Pyrolysis* **2016**, *120*, 37−44.

(4) Novak, J. M.; Ippolito, J. A.; Watts, D. W.; Sigua, G. C.; Ducey, T. F.; Johnson, M. G. *Biochar* **2019**, *1*, 97−114.

(5) Natasha, N.; Shahid, M.; Khalid, S.; Bibi, I.; Naeem, M. A.; Niazi, N. K.; Tack, F. M. G.; Ippolito, J. A.; Rinklebe, J. *Crit. Rev. Environ. Sci. Technol.* **2021**, 1−41 Ahead of Print.

(6) Xiang, L.; Liu, S.; Ye, S.; Yang, H.; Song, B.; Qin, F.; Shen, M.; Tan, C.; Zeng, C.; Tan, X. *J. Hazard. Mater.* **2021**, *420*, 126611 Ahead of print.

(7) Dieguez-Alonso, A.; Anca-Couce, A.; Zobel, N. *J. Anal. Appl. Pyrolysis* **2013**, *102*, 33−46.

(8) Dieguez-Alonso, A.; Anca-Couce, A.; Zobel, N.; Behrendt, F. *Fuel* **2015**, *153*, 102−109.

(9) Wang, C.; Wang, Y.; Herath, H. M. S. K. *Org. Geochem.* **2017**, *114*, 1−11.

(10) Tack, F. M. G.; Egene, C. E., Potential of biochar for managing metal contaminated areas, in synergy with phytomanagement or other management options. In *Biochar from Biomass and Waste*, Ok, Y. S., Ed. 2019; pp. 91−111.

(11) Smith, C. R.; Buzan, E. M.; Lee, J. W. *ACS Sustainable Chem. Eng.* **2013**, *1*, 118−126.

(12) Rombolà, A. G.; Meredith, W.; Snape, C. E.; Baronti, S.; Genesio, L.; Vaccari, F. P.; Miglietta, F.; Fabbri, D. *Environ. Sci. Technol.* **2015**, *49*, 11037−11044.

(13) Rombolà, A. G.; Fabbri, D.; Meredith, W.; Snape, C. E.; Dieguez-Alonso, A. *J. Anal. Appl. Pyrolysis* **2016**, *121*, 230−239.

(14) Wozniak, A. S.; Goranov, A. I.; Mitra, S.; Bostick, K. W.; Zimmerman, A. R.; Schlesinger, D. R.; Myneni, S.; Hatcher, P. G. *Org. Geochem.* **2020**, *148*, 104065.

(15) Bonanomi, G.; Ippolito, F.; Cesarano, G.; Vinale, F.; Lombardi, N.; Crasto, A.; Woo, s. L.; Scala, F. *Appl. Soil Ecol.* **2018**, *124*, 351−361.

(16) Wong, J. W. C.; Webber, J. B. W.; Ogbonnaya, U. O. *J. Anal. Appl. Pyrolysis* **2019**, *143*, 104687.

(17) Ben, H.; Hao, N.; Liu, Q.; Ragauskas, A. J. *BioEnergy Res.* **2017**, *10*, 1036−1044.

(18) Li, X.; Shen, Q.; Zhang, D.; Mei, X.; Ran, W.; Xu, Y.; Yu, G. *PLoS One* **2013**, *8*, No. e65949.

(19) Le Brech, Y.; Delmotte, L.; Raya, J.; Brosse, N.; Gadiou, R.; Dufour, A. *Anal. Chem.* **2015**, *87*, 843−847.

(20) Knicker, H. *Biogeochemistry* **2007**, *85*, 91−118.

(21) Kögel-Knabner, I. *Soil Biol. Biochem.* **2002**, *34*, 139−162.

(22) Rodgers, R. P.; Marshall, A. G. Petroleomics: Advanced Characterization of Petroleum-Derived Materials Characterized by Fourier Transform Ion Cyclotron Resonance Mass Spectrometry (FT-ICR MS). In *Asphaltenes, Heavy Oils and Petroleomics*; Mullins, O. C., Sheu, E. Y., Hammami, A., Marshall, A. G., Eds.; Springer: New York, 2007.

(23) McKenna, A. M.; Williams, J. T.; Putman, J. C.; Aeppli, C.; Reddy, C. M.; Valentine, D. L.; Lemkau, K. L.; Kellermann, M. Y.; Savory, J. J.; Kaiser, N. K.; Marshall, A. G.; Rodgers, R. P. *Energy Fuels* **2014**, *28*, 2454−2464.

(24) Smith, C. R.; Sleighter, R. L.; Hatcher, P. G.; Lee, J. W. *Environ. Sci. Technol.* **2013**, *47*, 13294−13302.

(25) Bird, M. I.; Wynn, J. G.; Saiz, G.; Wurster, C. M.; McBeath, A. *Annu. Rev. Earth Planet. Sci.* **2015**, *43*, 273−298.
(26) Goranov, A. I.; Wozniak, A. S.; Bostick, K. W.; Zimmerman, A. R.; Mitra, S.; Hatcher, P. G. *Geochim. Cosmochim. Acta* **2020**, *290*, 271−292.
(27) Hilber, I.; Blum, F.; Leifeld, J.; Schmidt, H.-P.; Bucheli, T. D. *J. Agric. Food Chem.* **2012**, *60*, 3042−3050.
(28) Fabbri, D.; Rombolà, A. G.; Torri, C.; Spokas, K. A. *J. Anal. Appl. Pyrolysis* **20132013**, *103*, 60−67.
(29) Conti, R.; Fabbri, D.; Vassura, I.; Ferroni, L. *J. Anal. Appl. Pyrolysis* **2016**, *122*, 160−168.
(30) Chacón-Patiño, M. L.; Rowland, S. M.; Rodgers, R. P. *Energy Fuels* **2018**, *32*, 9106−9120.
(31) Jonker, M. T. O.; Koelmans, A. A. *Environ. Sci. Technol.* **2002**, *36*, 4107−4113.
(32) Dubroca, T.; Smith, A. N.; Pike, K. J.; Froud, S.; Wylde, R.; Trociewitz, B.; McKay, J.; Mentink-Vigier, F.; van Tol, J.; Wi, S.; Brey, W.; Long, J. R.; Frydman, L.; Hill, S. *J. Magn. Reson.* **2018**, *289*, 35−44.
(33) Mentink-Vigier, F.; Marin-Montesinos, I.; Jagtap, A. P.; Halbritter, T.; van Tol, J.; Hediger, S.; Lee, D.; Sigurdsson, S. T.; De Paëpe, G. *J. Am. Chem. Soc.* **2018**, *140*, 11013−11019.
(34) Duber, S.; Więekowski, A. B. *Fuel* **1982**, *61*, 433−436.
(35) He, C.; Fang, Z.; Li, Y.; Jiang, C.; Zhao, S.; Xu, C.; Zhang, Y.; Shi, Q. *Environ. Sci.: Processes Impacts* **2021**, *23*, 1466−1475.
(36) McKenna, A. M.; Purcell, J. M.; Rodgers, R. P.; Marshall, A. G. *Energy Fuels* **2009**, *23*, 2122−2128.
(37) Dittmar, T.; Koch, B. P. *Mar. Chem.* **2006**, *102*, 208−217.
(38) Purcell, J. M.; Hendrickson, C. L.; Rodgers, R. P.; Marshall, A. G. *J. Am. Soc. Mass Spectrom.* **2007**, *18*, 1682−1689.
(39) Kanao, E.; Kubo, T.; Naito, T.; Matsumoto, T.; Sano, T.; Yan, M.; Otsuka, K. *Anal. Chem.* **2019**, *91*, 2439−2446.
(40) Joshi, Y. V.; Mennito, A. S.; Brown, S. H.; Qian, K. *Fuel* **2021**, *301*, 121066.
(41) Lobodin, V. V.; Marshall, A. G.; Hsu, C. S. *Anal. Chem.* **2012**, *84*, 3410−3416.
(42) Ruiz-Morales, Y. *J. Phys. Chem. A.* **2002**, *106*, 11283−11308.
(43) Ippolito, J. A.; Cui, L.; Kammann, C.; Wrage-Mönnig, N.; Estavillo, J. M.; Fuertes-Mendizabal, T.; Cayuela, M. L.; Sigua, G.; Novak, J.; Spokas, K.; Borchard, N. *Biochar* **2020**, *2*, 421−438.
(44) Patriarca, C.; Balderrama, A.; Može, M.; Sjöberg, P. J. R.; Bergquist, J.; Tranvik, L. J.; Hawkes, J. A. *Anal. Chem.* **2020**, *92*, 14210−14218.
(45) Shi, Q.; Zhao, S.; Xu, Z.; Chung, K. H.; Zhang, Y.; Xu, C. *Energy Fuels* **2010**, *24*, 4005−4011.
(46) Zhang, Y.; Xu, C.; Shi, Q.; Zhao, S.; Chung, K. H.; Hou, D. *Energy Fuels* **2010**, *24*, 6321−6326.
(47) Niles, S. F.; Chacón-Patiño, M. L.; Chen, H.; McKenna, A. M.; Blakney, G. T.; Rodgers, R. P.; Marshall, A. G. *Environ. Sci. Technol.* **2019**, *53*, 6887−6894 Just Accepted.
(48) Cole, D. P.; Smith, E. A.; Lee, Y. J. *Energy Fuels* **2012**, *26*, 3803−3809.
(49) Templier, J.; Miserque, F.; Barré, N.; Mercier, F.; Croué, J.-P.; Derenne, S. *J. Anal. Appl. Pyrolysis* **2012**, *97*, 62−72.
(50) Hertkorn, N.; Harir, M.; Cawley, K. M.; Schmitt-Kopplin, P.; Jaffé, R. *Biogeosciences* **2016**, *13*, 2257−2277.
(51) Koch, B. P.; Witt, M.; Engbrodt, R.; Dittmar, T.; Kattner, G. *Geochim. Cosmochim. Acta* **2005**, *69*, 3299−3308.

https://doi.org/10.1021/acs.analchem.1c03058
Anal. Chem. 2021, 93, 15365−15372